8

Time-Frequency Analysis of Micro-Doppler Phenomenon

When a radar transmits a signal to a target, the transmitted signal interacts with the target and returns back to the radar. The change in the property of the returned signal reflects characteristics of interest in the target. When the transmitted signal of a coherent Doppler radar hits a moving target, the wavelength of the signal will be changed, and the carrier frequency of the signal will be shifted, known as the Doppler effect. The Doppler frequency shift reflects the velocity of the moving target. When the target is moving away from the radar, the return signal will have a longer wavelength or negative Doppler shift; if the target is moving towards the radar, the return signal will have a shorter wavelength or positive Doppler shift. As we mentioned in Chapter 1, coherent radar systems can preserve phase information of the returned signal. From the obtained phase function of time, by taking the time derivative of the phase, Doppler shifts induced by targets' motions can be found.

An important application of the coherent radar is target identification. A target can be identified based on its signature (i.e., a distinctive characteristic that indicates identity of a target). Signature generated from radar targets' returns is called the radar signature of the target. Radar signature can be in the time domain, such as a range profile of a target, or in the frequency domain, such as the spectrum of a range profile. In this chapter, we will introduce radar signature in a joint time-frequency domain. The time-frequency signature is especially useful to catch time-dependent frequency characteristics.

Mechanical vibration or rotation of structures on a target may induce frequency modulation on the returned radar signal and generates sidebands about the Doppler frequency shift of the target's body. The modulation due to vibrations is called the micro-Doppler phenomenon, originally introduced in coherent laser radar or ladar systems [1, 2]. Because ladar uses the same principle as radar, we adopt it here for radar applications. The modulation induced by rotations, which can be seen as a special case of vibration, can also be interpreted as micro-Doppler. The micro-Doppler phenomenon can be regarded as a characteristic of the interaction between the vibrating or rotating structures and the target body. The change of the properties of back-scattering enables us to determine some properties of the target, and thus the target of interest can be identified based on its micro-Doppler signature. The micro-Doppler provides an additional piece of information for target recognition that is complementary to existing recognition methods [3].

In this chapter, we examine the use of time-frequency analysis for the micro-Doppler phenomenon. In Section 8.1, we analyze micro-Doppler induced by a vibrating scattering center, illustrate time-frequency signature of a vibrating point-scatterer using radar-measured data, and demonstrate time-frequency signature of micro-Doppler generated by the swinging arms of a walking man. In Section 8.2, we introduce micro-Doppler induced by rotation structures and examine the important example of rotor blades. We review the time-domain and the frequency-domain signatures of radar returns from rotor blades, and introduce the time-frequency signatures of rotor blades using both simulated and measured radar data.

8.1 Vibration-Induced Micro-Doppler

In a coherent radar, the phase of a signal returned from a target is sensitive to the variation in range. A half-wavelength change in range can cause 360-degree phase change. It is conceivable that the vibration of a reflecting surface may be measured with the phase change. Thus, the Doppler frequency shift, which represents the change of phase with time, can be used to detect vibrations of structures on a target [3]. These characteristics of vibration are useful for detection and recognition of targets.

Figure 8.1 illustrates a radar located at the origin of the radar coordinate system (X, Y, Z) and a point-scatterer P vibrating about a center point Q that is also the origin of reference coordinates (x, y, z) translated from (X, Y, Z) and at a distance R_0 from the radar. We assume that the center
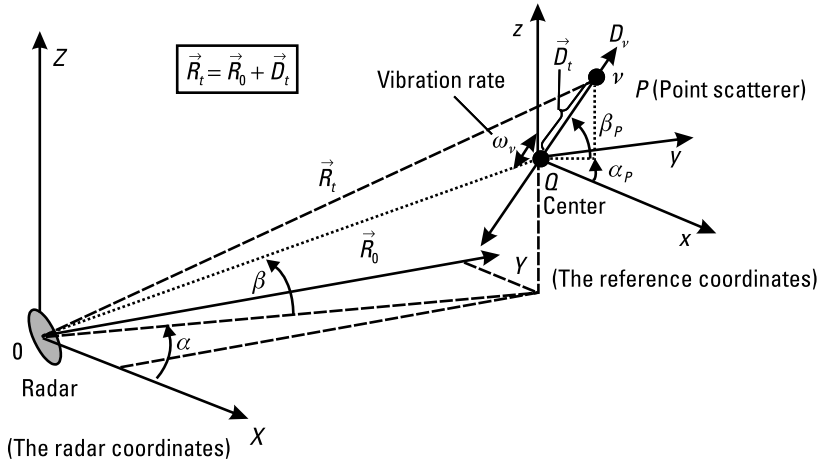
Figure 8.1 Geometry of the radar and a vibrating reflector.

point Q is stationary with respect to the radar. If the azimuth and elevation angles of the point Q with respect to the radar are α and β, respectively, the point Q is located at $(R_0 \cos\beta \cos\alpha, R_0 \cos\beta \sin\alpha, R_0 \sin\beta)$ in the (X, Y, Z) coordinates. We assume that the scatterer P is at a distance D_t from the center point Q and that the azimuth and elevation angles of the scatterer P with respect to the center point Q are α_P and β_P, respectively. Then, the scatterer P will be located at $(D_t \cos\beta_P \cos\alpha_P, D_t \cos\beta_P \sin\alpha_P, D_t \sin\beta_P)$ in the reference coordinates (x, y, z). Therefore, the vector from the radar to the scatterer P becomes $\vec{R}_t = \vec{R}_0 + \vec{D}_t$ as shown in Figure 8.1. The range from the radar to the scatterer P can be expressed as

$$R_t = \left|\vec{R}_t\right| = [(R_0 \cos\beta \cos\alpha + D_t \cos\beta_P \cos\alpha_P)^2$$
$$+ (R_0 \cos\beta \sin\alpha + D_t \cos\beta_P \sin\alpha_P)^2 \qquad (8.1)$$
$$+ (R_0 \sin\beta + D_t \sin\beta_P)^2]^{1/2}$$

When $R_0 \gg D_t$, the range is approximately

$$R_t = \{R_0^2 + D_t^2 + 2R_0 D_t [\cos\beta \cos\beta_P \cos(\alpha - \alpha_P) + \sin\beta \sin\beta_P]\}^{1/2}$$
$$\approx R_0 + D_t [\cos\beta \cos\beta_P \cos(\alpha - \alpha_P) + \sin\beta \sin\beta_P] \qquad (8.2)$$

In the case that the azimuth angle α of the center point Q and the elevation angle β_P of the scatterer P are all zero, if $R_0 \gg D_t$ we have

$$R_t = (R_0^2 + D_t^2 + 2R_0 D_t \cos\beta \cos\alpha_P)^{1/2} \cong R_0 + D_t \cos\beta \cos\alpha_P$$

If the vibration rate of the scatterer in angular frequency is ω_v and the amplitude of the vibration is D_v, then $D_t = D_v \sin\omega_v t$ and the range of the scatterer becomes

$$R(t) = R_t = R_0 + D_v \sin\omega_v t \cos\beta \cos\alpha_P \qquad (8.3)$$

Thus, the radar received signal becomes

$$s_R(t) = \rho\exp\left\{j\left[2\pi f_0 t + 4\pi\frac{R(t)}{\lambda}\right]\right\} = \rho\exp\{j[2\pi f_0 t + \Phi(t)]\}$$
$$(8.4)$$

where ρ is the reflectivity of the point-scatterer, f_0 is the carrier frequency of the transmitted signal, λ is the wavelength, and $\Phi(t) = 4\pi R(t)/\lambda$ is the phase function.

Substituting (8.3) into (8.4) and denoting $B = (4\pi/\lambda)D_v \cos\beta \cos\alpha_P$, the received signal can be rewritten as

$$s_R(t) = \rho\exp\left\{j\frac{4\pi}{\lambda}R_0\right\}\exp\{j2\pi f_0 t + B\sin\omega_v t\} \qquad (8.5)$$

which can be further expressed by the Bessel function of the first kind of order k:

$$J_k(B) = \frac{1}{2\pi}\int\limits_{-\pi}^{\pi}\exp\{j(B\sin u - ku)du\} \qquad (8.6)$$

and, thus,

$$s_R(t) = \rho\exp\left(j\frac{4\pi}{\lambda}R_0\right)\sum_{k=-\infty}^{\infty}J_k(B)\exp[j(2\pi f_0 + k\omega_v)t]$$

$$= \rho\exp\left(j\frac{4\pi}{\lambda}R_0\right)\{J_0(B)\exp(j2\pi f_0 t) \qquad (8.7)$$

$$+ J_1(B)\exp[j(2\pi f_0 + \omega_v)t] - J_1(B)\exp[j(2\pi f_0 - \omega_v)t]$$
$$+ J_2(B)\exp[j(2\pi f_0 + 2\omega_v)t] + J_2(B)\exp[j(2\pi f_0 - 2\omega_v)t]$$
$$+ J_3(B)\exp[j(2\pi f_0 + 3\omega_v)t] - J_3(B)\exp[j(2\pi f_0 - 3\omega_v)t]$$
$$+ \dots\}$$

Therefore, the micro-Doppler frequency spectrum consists of pairs of spectral lines around the center frequency f_0 and with spacing $\omega_v/(2\pi)$ between adjacent lines.

By taking the time-derivative of the phase function in (8.4), the micro-Doppler frequency induced by the vibration is a sinusoidal function of time at the vibration frequency ω_v:

$$f_D = \frac{1}{2\pi}\frac{d\Phi}{dt} = \frac{2}{\lambda}\frac{dR(t)}{dt} \tag{8.8}$$

$$= \frac{2}{\lambda}D_v\omega_v[\cos\beta\cos\beta_P\cos(\alpha - \alpha_P) + \sin\beta\sin\beta_P]\cos\omega_v t$$

If the azimuth angle and the elevation angle β_P are all zero, we have

$$f_D = \frac{2}{\lambda}D_v\omega_v\cos\beta\cos\alpha_P\cos\omega_v t \tag{8.9}$$

When the orientation of the vibrating scatterer is along the projection of the radar LOS direction, or $\alpha_P = 0$, and the elevation angle β of the scatterer is also 0, the Doppler frequency change reaches the maximum value of $(2/\lambda)D_v\omega_v$.

Usually, when the vibrating modulation is small, it is difficult to detect the vibration in the frequency domain. Thus, a method that removes the energy of the target's Doppler velocity and keeps only the residual Doppler (i.e., the micro-Doppler), may help distinguish vibration spectrum from other contributions.

8.1.1 Time-Frequency Signature of a Vibrating Scatterer

According to (8.9), when a radar is operating at X-band with a wavelength of 3 cm, a vibration rate at 10 Hz with a displacement of 0.1 cm will induce a maximal micro-Doppler frequency shift of 0.66 Hz as shown in Figure 8.2. The micro-Doppler shift may be detectable with a high frequency-resolution radar. This is illustrated by analyzing a time series collected using an X-band SF radar illuminating two point-scatterers shown in Figure 8.3(a). The two scatterers are separated by a distance of 13.5 m. One scatterer is stationary and the other is vibrating at 1.5 Hz with a displacement of 3 cm [4]. Although the vibration rate is relatively low, according to (8.9) the displacement of 3 cm can still generate larger micro-Doppler frequency shift up to 3 Hz. Figure 8.3(b) is the magnitude of the I and Q returned signals
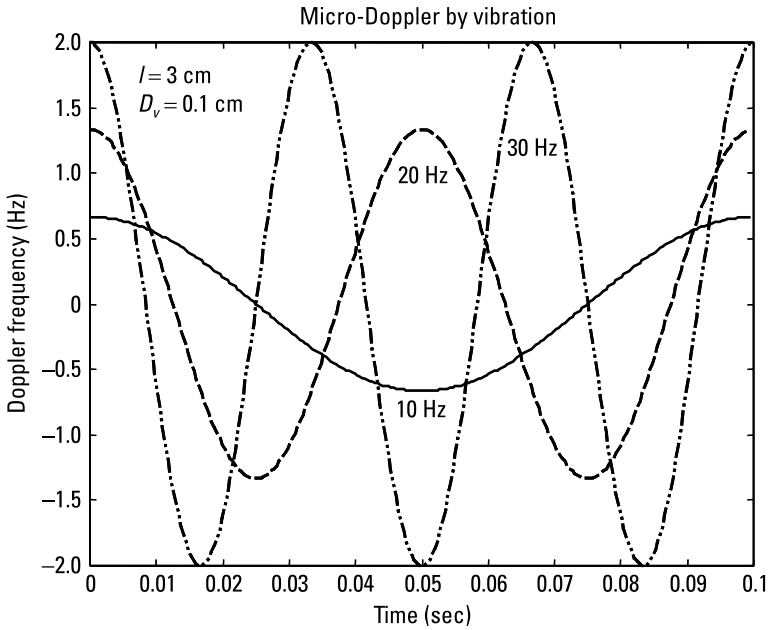
Figure 8.2 Micro-Doppler generated by a vibrating reflector with a vibration rate of 10 Hz, 20 Hz, and 30 Hz, respectively.

from the two scatterers during a short time interval. By taking the Fourier transform of the I and Q signals, the magnitude of its Fourier frequency spectrum has one sharp peak around 0.29 and one peak spread around 0.35 to 0.39 as shown in Figure 8.3(c), where the maximum frequency scale is normalized to 0.5. As we described in Chapter 1, for an SF radar waveform, which sequentially transmits short rectangular pulses with a carrier frequency stepped from one pulse to the next, the pulse compression is performed by the Fourier transform. By taking the Fourier transform, the radar received SF signal can be compressed and appears as a radar "range profile." In other words, the Fourier spectrum in Figure 8.3(c) is actually a "range profile," where the two peaks represent the two point-scatterers located in range. The peak spread in the spectrum indicates that there may be a modulation due to vibrating. However, the width of the peak measured from the spectrum does not reflect the true displacement of the vibrating scatterer because the "range profile" is actually the Fourier spectrum in the frequency-domain.

Figure 8.3(d) shows the time-frequency signature of the radar signal returned from the two scatterers, where the vibration curve can be observed very well. It is obtained by applying a Gabor transform described in Chapter 2.
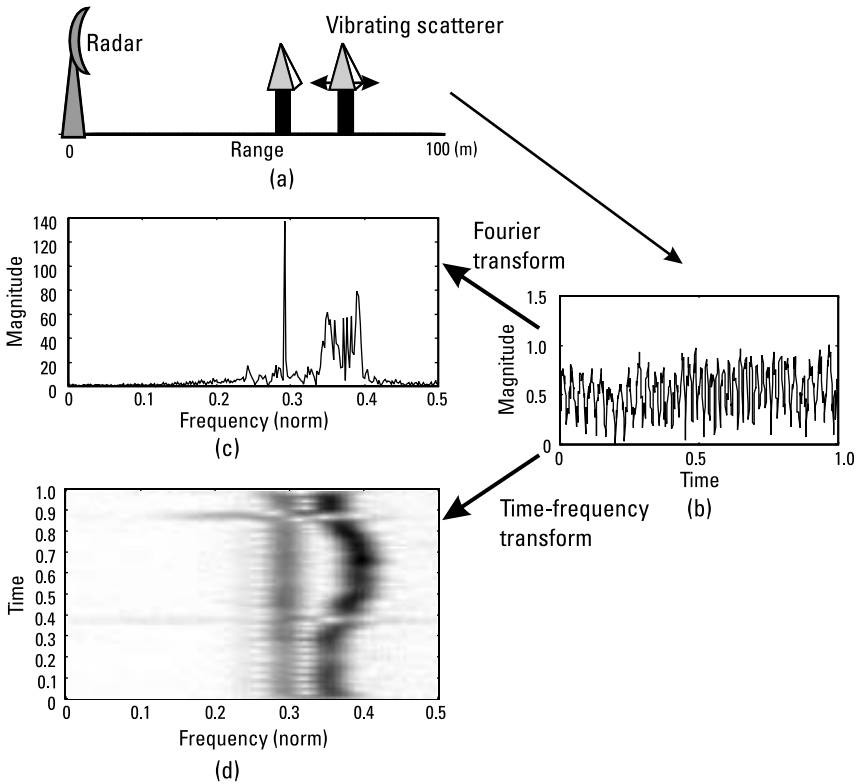
Figure 8.3 An experimental radar-returned signal from two point-scatterers: (a) geometry of the radar and the two scatterers; (b) the magnitude of the radar-returned signal; (c) the Fourier transform of the radar-returned signal; and (d) the time-frequency transform of the returned signal. (Data provided by S. Wong, DREO of Canada.)

From the time-frequency signature we can see that the micro-Doppler of the vibrating scatterer is a time-varying frequency spectrum. From the additional time information, it is possible to estimate the vibration rate of the vibrating scatterer by measuring the period of the vibration curve. However, the maximum displacement of the vibration curve does not reflect the true displacement in range, as mentioned earlier.

8.1.2 An Example of Micro-Doppler Signatures of Moving Targets

Here we demonstrate an example of micro-Doppler signatures of moving targets. The moving target in this example is a walking man with swinging

arms. The radar is mounted on the rooftop of a building, and a man is walking towards the building at a speed of about 1.8 m/sec as illustrated in Figure 8.4(a). The radar data has 64 range cells and 1,000 pulses and was collected at a PRF of 800 Hz. Figure 8.4(b) shows radar-range and cross-range images of the walking man generated by 64 range-cells and 128 pulses, where the hot spot in the image indicates the body of the walking man. We also notice that there are smeared lines running across the cross-range direction around the body of the walking man at the range cell 12. If we apply a Gabor transform to the time history data at the range cell 12, the body Doppler shift and the micro-Doppler signature of the swinging arms can be clearly detected in the time-frequency domain [4]. As shown in Figure 8.4(c), the Doppler shift of one arm is higher and the other is lower than the body Doppler frequency shift. Figure 8.4(d, e) shows the result with
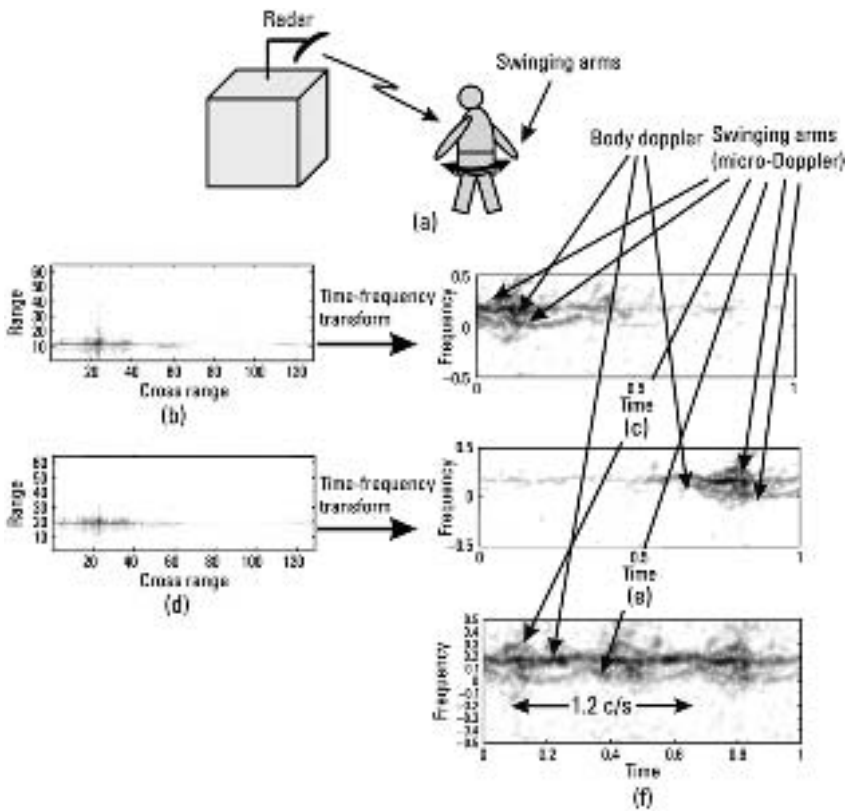

Figure 8.4 Time-frequency signatures of a walking man with swinging arms. (Data provided by H. Holt, Norden Systems, Northrop Grumman.)

the same data but in a different short-time interval and at the range cell 20. Superposition of the time-frequency signatures over several range cells, which correspond to different walking steps, gives a full time-frequency signature of the walking man as shown in Figure 8.4(f). We can see that the body's Doppler shift is almost constant but the arm's micro-Doppler shift becomes time-varying and has a sinusoidal-like curve. Again, from the additional time information, the swinging rate of the arm can be estimated and is about 1.2 cycle/sec in this example.

8.2 Rotation-Induced Micro-Doppler

Modulation induced by rotation structure (such as rotor blades of a helicopter, propellers of an aircraft, or rotating antennas on a ship or an aircraft) can be regarded as a unique signature of the target. The micro-Doppler signature becomes an important feature for identifying the target of interest. Here, we examine micro-Doppler induced by rotor blades of a helicopter, show the time-domain and the frequency-domain signatures of the micro-Doppler, and introduce the time-frequency signature of the micro-Doppler induced by rotor blades.

8.2.1 Rotor Blade Motion

In a helicopter, the main rotor blades, the tail rotor blades, and the hub have unique signatures suitable for target identification. Generally, radar returns from a helicopter are back-scattered from the fuselage, the rotor blades, the tail blades, the hub, and other structures on the helicopter. The motion of the rotor blades depends on the interdependent coupling between the aerodynamics and the rotor dynamics [5]. Each blade is a rotating aerofoil having bending, flexing, and twisting. The radar cross section of a segment in the blade depends upon its distance from the center of rotation, its angular position, and the aspect angle of the rotor [6, 7].

Because we are especially interested in electromagnetic back-scattering from the main rotating blades of a helicopter, for simplicity, the rotor blade is modeled as a rigid, homogeneous, and linear rod rotating about a fixed axis with a constant rotation rate. No flapping, lagging, and feathering are considered for the calculation of electromagnetic back-scattering.

8.2.2 Radar Returns from Rotor Blades

As illustrated in Figure 8.5, the radar is located at the origin of the radar coordinates (X, Y, Z); reference coordinates (x, y, z) are translated from
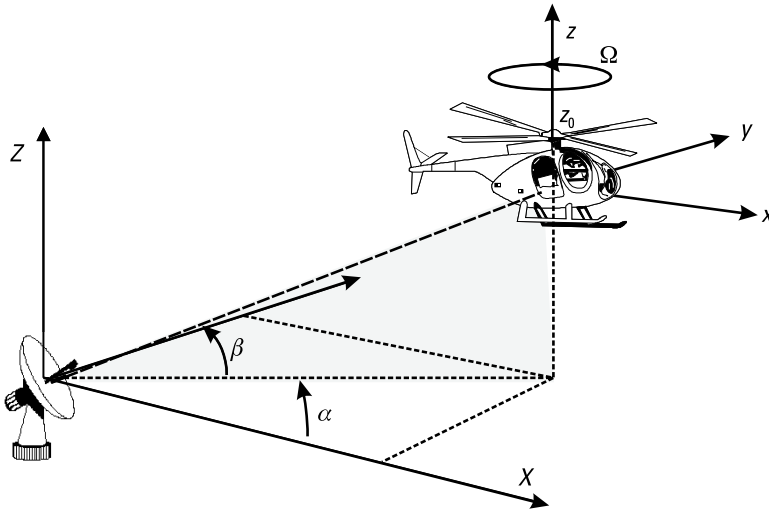
Figure 8.5 Geometry of the radar and the helicopter.

the radar coordinates and their origin is at the geometric center of the helicopter. The rotor blades are on the plane $(x, y, z = z_0)$ and rotate about the z-axis with a rotation rate of Ω. The azimuth and the elevation angles of the helicopter with respect to the radar are α and β, respectively.

Let us begin with a simple case where $\alpha = \beta = 0$ and $z_0 = 0$ as shown in Figure 8.6. Assume a scatterer P at (x_0, y_0) on a rotor blade rotates about a center point Q with a rotation rate of Ω. The distance from the scatterer to the center point is l, and the distance between the radar and the center point is R_0, which may be a function of time if the target is moving. Assume that at $t = 0$ the initial rotation angle of the scatterer in the blade is θ_0, and at t the rotation angle becomes $\theta_t = \theta_0 + \Omega t$ and the scatterer is rotated to
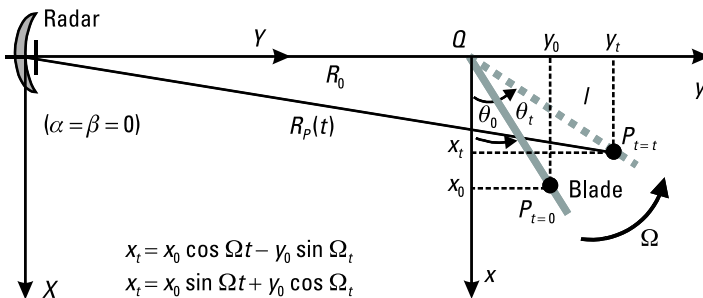

Figure 8.6 Geometry of the radar and a rotor blade when $\alpha = \beta = 0$.

(x_t, y_t). Because we assume both the radar and the rotor are on the same plane, at time t the range from the radar to the scatterer can be derived as

$$R_P(t) = [R_0^2 + l^2 + 2lR_0 \sin(\theta_0 + \Omega t)]^{1/2} \tag{8.10}$$
$$\cong R_0 + V_R t + l \sin \theta_0 \cos \Omega t + l \cos \theta_0 \sin \Omega t$$

where V_R is the radial velocity of the helicopter and $(l/R_0)^2 \to 0$ for far field. Thus, the radar received signal becomes

$$s_R(t) = \exp\left\{ j\left[2\pi f_0 t + \frac{4\pi}{\lambda} R_P(t) \right] \right\} = \exp\{j[2\pi f_0 t + \Phi_P(t)]\} \tag{8.11}$$

where $\Phi_P(t) = 4\pi R_P(t)/\lambda$ is the phase function.

If the elevation angle β and the height of rotor blades z_0 are not zero, then the phase function should be modified as

$$\Phi_P(t) = \frac{4\pi}{\lambda} [R_0 + V_R t + \cos\beta(l\sin\theta_0 \cos\Omega t + l\cos\theta_0 \sin\Omega t) + z_0 \sin\beta] \tag{8.12}$$

The returned signal from the scatterer P in the rotor blade becomes

$$s_R(t) = \exp\left\{ j\frac{4\pi}{\lambda} [R_0 + V_R t + z_0 \sin\beta] \right\} \tag{8.13}$$
$$\cdot \exp\left\{ j2\pi f_0 t + \frac{4\pi}{\lambda} l \cos\beta \sin(\Omega t + \theta_0) \right\}$$

Let $\theta_0 = 0$, denote B $= (4\pi/\lambda)l\cos\beta$, and reduce (8.13) to (8.5). Again, it can be expressed by the Bessel function of the first kind. Similar to (8.7), the micro-Doppler of a scatterer on the blade consists of pairs of spectral lines around the center frequency f_0 and with spacing $\Omega/(2\pi)$ between adjacent lines.

After compensating the motion and removing the constant phase term in (8.13), the baseband signal returned from the scatterer P becomes

$$s_B(t) = \exp\left\{ j\frac{4\pi}{\lambda} l \cos\beta \sin(\Omega t + \theta_0) \right\} \tag{8.14}$$

By integrating (8.14) over the length of the blade L, the total baseband signal becomes the following [6]:

$$s_L(t) = \int_0^L \exp\left\{ j\frac{4\pi}{\lambda} l\cos\beta \sin(\Omega t + \theta_0) \right\} dl \tag{8.15}$$

$$= L\exp\left\{ j\frac{4\pi}{\lambda}\frac{L}{2}\cos\beta \sin(\Omega t + \theta_0) \right\} \text{sinc}\left\{ \frac{4\pi}{\lambda}\frac{L}{2}\cos\beta \sin(\Omega t + \theta_0) \right\}$$

For a rotor with N blades, there will be N different initial rotation angles

$$\theta_k = \theta_0 + k2\pi/N, \ (k = 0, 1, 2, \ldots N - 1) \tag{8.16}$$

and the total received signal becomes

$$s_\Sigma(t) = \sum_{k=0}^{N-1} s_{Lk}(t) \tag{8.17}$$

$$= \sum_{k=0}^{N-1} L\,\text{sinc}\left\{ \frac{4\pi}{\lambda}\frac{L}{2}\cos\beta \sin(\Omega t + \theta_0 + k2\pi/N) \right\} \exp\{j\Phi_k(t)\}$$

where

$$\Phi_k(t) = \frac{4\pi}{\lambda}\frac{L}{2}\cos\beta \sin(\Omega t + \theta_0 + k2\pi/N) \quad (k = 0, 1, 2, \ldots N - 1) \tag{8.18}$$

8.2.3 Time-Domain Signatures of Rotation-Induced Modulations

Rotor blades in a helicopter are in rotational motion that will impart a periodic modulation on radar returned signals as shown in (8.17). The rotation-induced Doppler shifts relative to the Doppler shift of the fuselage (or body) occupy unique locations in the frequency domain. The modulation in the frequency domain as well as the time-domain signal have been used as radar signatures for target identification [8, 9].

The time-domain signature of rotor blades is defined by the magnitude in (8.17)

$$\left| s_\Sigma(t) \right| = \left| \sum_{k=0}^{N-1} L \operatorname{sinc}\left\{ \frac{4\pi}{\lambda} \frac{L}{2} \cos\beta \sin(\Omega t + \theta_0 + k2\pi/N) \right\} \exp\{j\Phi_k(t)\} \right| \tag{8.19}$$

where $\Phi_k(t)$ is defined by (8.18).

Assume a radar is operating at S-band with a wavelength of 0.1m, and a helicopter has 2 rotor blades at a constant rotation rate of 5 revolutions/sec (rev/sec). If the distance of the blade roots from the rotor center is 0.3m, the distance of the blade tips from the rotor center is 6.7m, and the elevation angle of the rotor $\beta = 0$, the time-domain signature of the rotor blades in (8.19) is shown in Figure 8.7(a). The frequency spectrum of the same signal is shown in 8.7(b), which we will discuss in Section 8.2.4. The rotor blade's return has a short flash when the blade has specular reflection at the advancing as well as at the receding point of rotation [9]. The interval between flashes is related to the rotation rate of the rotor. The duration of the flash is determined by the length of the blade L, the wavelength λ, and the rotation rate Ω as described by the sinc function in (8.19).
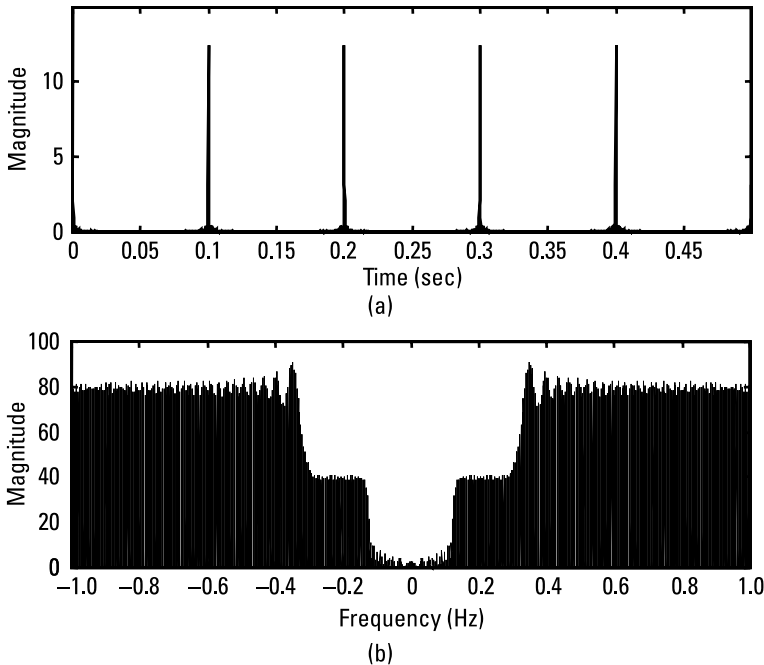

Figure 8.7 (a) The magnitude of the radar-returned signal from two rotor blades; and (b) the frequency spectrum of the radar-returned signal.

For longer blade length and at a shorter wavelength, the duration of the flash is shorter. Because the number of blades is 2 and the rotation rate is 5 rev/sec, there are 5 flashes in 0.5 sec, and the interval between flashes is 0.1 sec as shown in Figure 8.7(a).

Figure 8.8(a) shows a simple Computer-Aided Design (CAD) model of a helicopter with four rotor blades. An electromagnetic prediction code *Xpatch* was used to simulate radar returns from the helicopter model [10, 11]. The body of the helicopter is made by two conducting-boxes with different sizes. The length of the rotor blade is 3m. In the simulation, the radar scattering is observed at 128 frequency steps from 1.75 GHz to 2.25 GHz and 128 target aspect looks from 158 to 170 degrees. The elevation angle of the helicopter is 20 degrees. The blade position is articulated between 0 and 360 degrees during the 128 angular looks. The rotational motion of the helicopter's body is 12 rev/m or 0.2 rev/sec. The rotation rate of the rotor blade is 360 rev/m or 6 rev/sec [12]. Figure 8.8(b) is the standard radar image of the helicopter in the range versus cross-range domain by taking the 2D Fourier transform of the *Xpatch*-generated data. We can see that the body of the helicopter has a small extent around the center of the cross-range while the fast rotating rotor blades exhibit strong smeared lines running across the cross-range and overlapping with the body of the helicopter. The time-domain signature of the simulated helicopter is shown in Figure 8.9(a), where the radar signal includes returns from both the rotor blades and the helicopter body. The frequency spectrum of the same simulated helicopter is shown in 8.9(b), which will be discussed in Section 8.2.4.
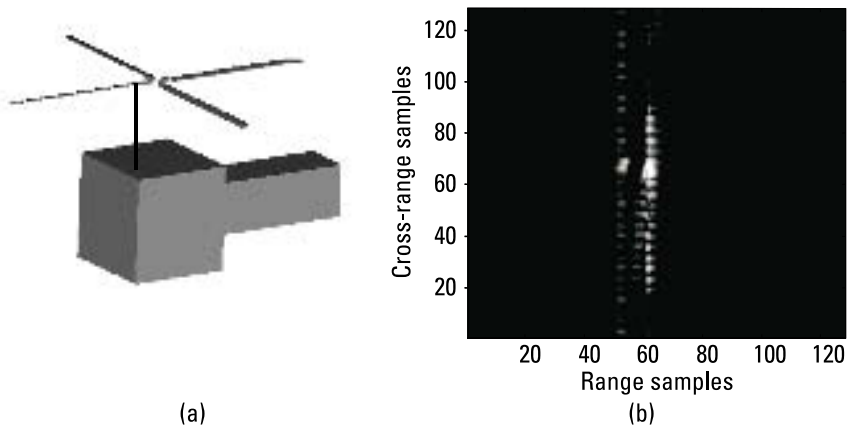

(a)   (b)

Figure 8.8 (a) A simplified CAD model of a helicopter with four rotor blades; and (b) the radar range and cross-range image of the helicopter.
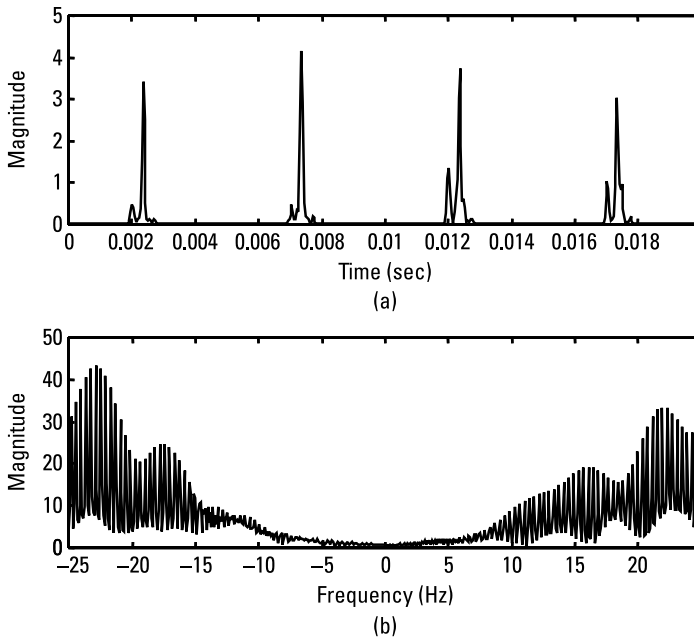
Figure 8.9 (a) The magnitude of the radar-returned signal from the simplified CAD model of a helicopter; and (b) the frequency spectrum of the radar-returned signal.

Figure 8.10(a) shows a similar time-domain signature of measured helicopter data. The overlapped range profiles illustrated in Figure 8.11 show separated flash peaks of rotor blades. It also shows overlapped peaks of returns from the body of the helicopter. Unlike the flash peaks, these overlapped body peaks are located at a fixed range cell. The corresponding frequency spectrum of the measured helicopter data is shown in 8.10 (b), which will be discussed in Section 8.2.4.

As was defined in Chapter 1, for each transmitted pulse, the time-domain signature is actually a range profile. From only one range profile, it is difficult to observe the rotation feature of rotor blades. However, owing to the frequency modulation induced by rotational motions, the rotation feature may be observed from the frequency-domain signature in its Doppler spectrum. To better observe the rotation feature of rotor blades, we use a sequence of range profiles by transmitting a sequence of pulses and rearranging them into a 2D (the range versus the dwell time) array matrix. At each range cell, the time history series across the range profiles provides a better way to observe the rotation behavior during a longer time period. This will be further discussed in Section 8.2.5.
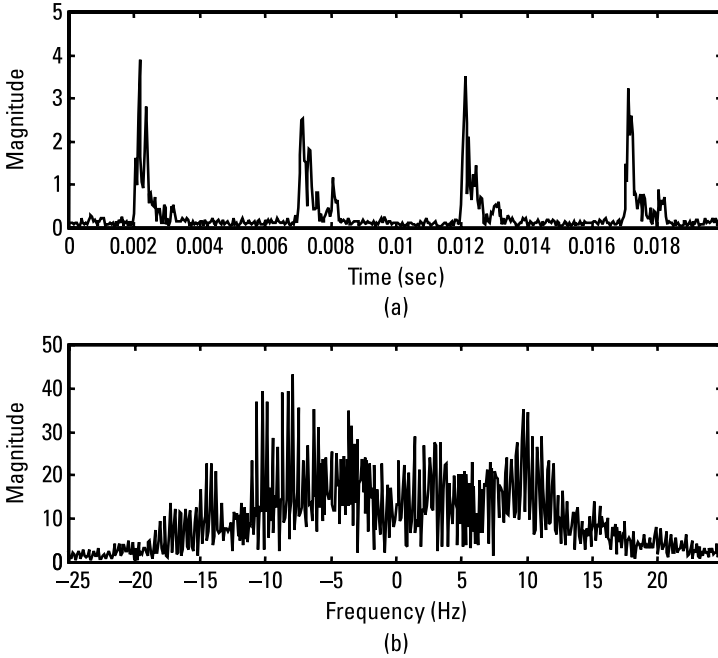
Figure 8.10 (a) The magnitude of the radar-returned signal from a helicopter; and (b) the frequency spectrum of the radar-returned signal.

8.2.4 Frequency-Domain Signatures

Because the time-derivative of the phase is the frequency, by taking the time-derivative of the phase function $\dfrac{4\pi}{\lambda}\dfrac{L}{2}\cos\beta\sin(\Omega t + \theta_0)$ in (8.15), the Doppler frequency shift induced by a rotor blade becomes

$$f_D(t) = \frac{L}{\lambda}\Omega\cos\beta(-\sin\theta_0\sin\Omega t + \cos\theta_0\cos\Omega t) \qquad (8.20)$$

If the initial rotation angle $\theta_0 = 0$, then we have $f_D(t) = \dfrac{L}{\lambda}\Omega\cos\beta\cos\Omega t$. We can clearly see that the Doppler frequency is modulated by the rotation rate Ω through $\cos\Omega t$. The frequency spectrum of the received signal can be directly obtained by taking the Fourier transform of (8.15).

For a rotor with N blades, the frequency spectrum of the total received baseband signal in (8.17) can be expressed as follows [6]:
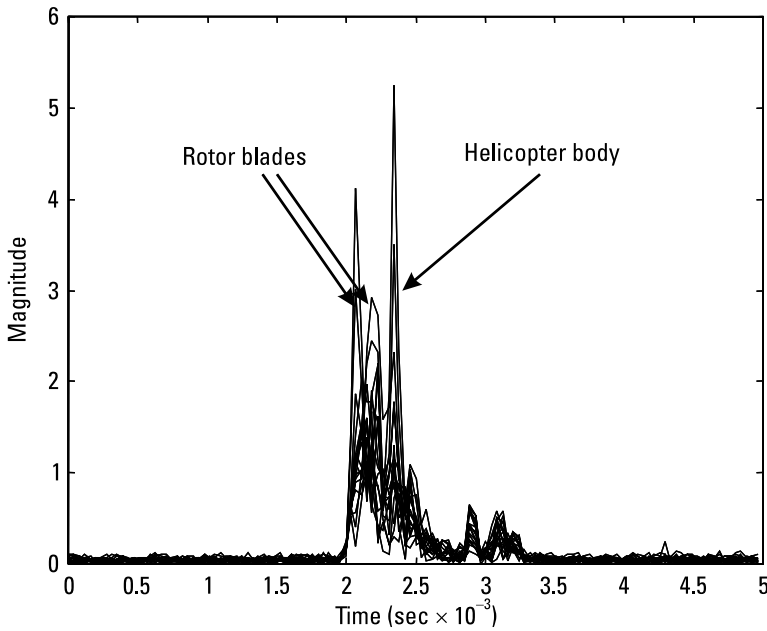
Figure 8.11 Overlapped individual range profiles of the measured radar data of a helicopter.

$$S_\Sigma(f) = \sum_{m=-M}^{M} C_m \delta(f - mN\Omega) \qquad (8.21)$$

where C_m is a scale factor determined by Bessel functions of the first kind with parameters of λ, L, β, N, and m, and M is the index number of the most significant sideband. Because we have compensated the translational motion of the rotor blades and removed the carrier frequency and the constant phase term, the residual frequency spectrum reflects only the micro-Doppler shifts induced by rotor blades relative to the zero frequency.

Figure 8.7(b) shows the frequency spectrum of radar returns from only the rotor blades and based on the baseband time-domain signal derived in (8.17). The Doppler modulation about center (zero) frequency can be seen. The lower cutoff frequency is determined by the distance between the rotor center and the blade roots. For the *Xpatch*-simulated radar data described in Section 8.2.3, the radar return is not only from rotor blades, but also from the body of the helicopter. The frequency spectrum of the data is shown in Figure 8.9(b), where the Doppler modulation about the center (zero) frequency can also be seen. For the measured radar data described in

Section 8.2.3, radar returns also include returns from structures other than rotor blades of the helicopter. The frequency signature is shown in Figure 8.10(b), where the Doppler frequency modulation about the center (zero) frequency can also be seen. However, due to noise spectrum, the magnitude of the spectrum around the center frequency is higher.

Frequency-domain signatures provide information about frequency modulations by either rotating blades or other rotating or vibrating structures. Because of the lack of time information, it is not easy to tell the rotation rate from the frequency spectrum alone. Therefore, the time-frequency signature that provides time-dependent frequency information is more useful as an additional information for target identification complementary to existing time-domain or frequency-domain methods.

8.2.5   Time-Frequency Signatures

Figure 8.12 illustrates a stack of radar range profiles of a helicopter. In each range profile, we assume that there are returns from four rotor blades and one return from the body of the helicopter. Because of the blades' rotation, the amplitudes of the blades' returns change from one profile to the next as seen in Figure 8.12. Thus, four blades have flashes at different times.
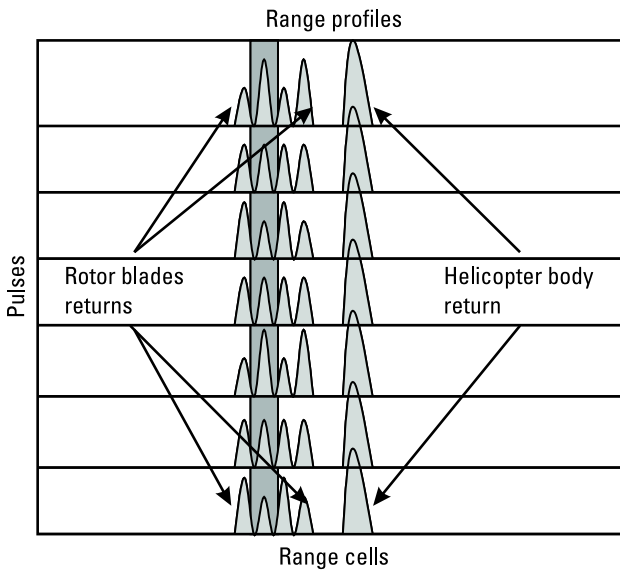

Figure 8.12   A stack of radar range profiles returned from a helicopter.

However, the amplitude of the return from the body is relatively stable. When we apply the Fourier transform to form an image of the helicopter, the image of the body is relatively clear but the image of the rotor blades is smeared along the cross-range domain.

Although range profiles can provide features, such as the location and the reflectivity of a scatterer, a better way to extract useful features of rotor blades may not be from the range profile. Instead, the data across range profiles at a range cell where the smearing in the cross-range occurs may be used. To extract features of rotor blades, we observe the time-frequency behavior of rotor blades by taking a time-frequency transform of the data across range profiles.

Figure 8.13 shows the time-frequency signature of the returned signal from the *Xpatch*-simulated helicopter shown in Figure 8.8, where the characteristics of the rotating blades can be seen more clearly in the joint time-frequency domain. The strong time-frequency distribution along the horizontal line about the center frequency is due to returns from the helicopter's body. The strong time-frequency distribution along slope-lines about
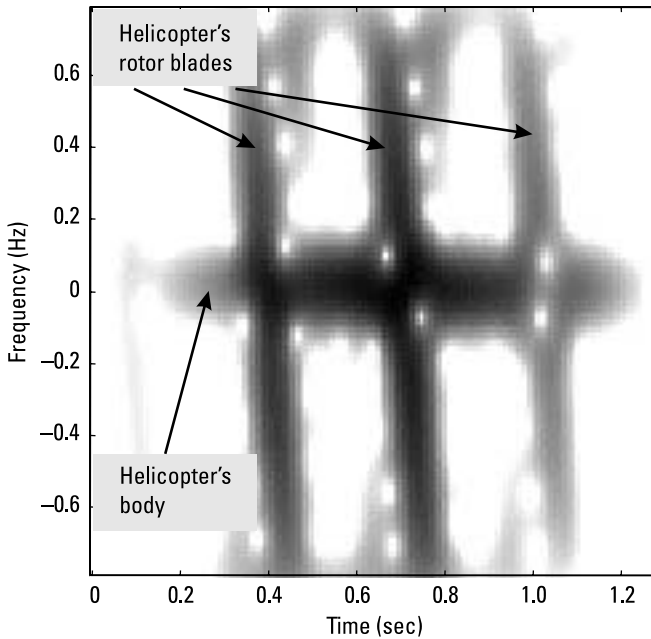

Figure 8.13 Time-frequency signature of the simulated radar-returned signal from the simplified CAD model of a helicopter.

the vertical direction is due to returns from the rotating blades. Because time information is now available, the rotation rate of the blades can be measured from their time-frequency signatures [13].

References

[1]   Parker, K. J., R. M. Lerner, and S. R. Huang, "Method and Apparatus for Using Doppler Modulation Parameters for Estimation of Vibration Amplitude," *U.S. Patent 5,086,775*, February 11, 1992.

[2]   Zediker, M. S., R. R. Rice, and J. H. Hollister, "Method for Extending Range and Sensitivity of a Fiber Optic Micro-Doppler Ladar System and Apparatus Therefor," *U.S. Patent 6,847,817*, December 8, 1998.

[3]   Sommer, H., and J. Salerno, "Radar Target Identification System," *U.S. Patent 3,614,779*, October 19, 1971.

[4]   Chen, V. C., "Analysis of Radar Micro-Doppler Signature with Time-Frequency Transform," *Proc. Tenth IEEE Workshop on Statistical Signal and Array Processing*, August 2000, pp. 463–466.

[5]   Leishman, J. G., *Principles of Helicopter Aerodynamics*, Cambridge University Press, 2000.

[6]   Martin, J., and B. Mulgrew, "Analysis of the Theoretical Radar Return Signal from Aircraft Propeller Blades," *IEEE International Radar Conference*, 1990, pp. 569–572.

[7]   Fliss, G. G., and D. L. Mensa, "Instrumentation for RCS Measurements of Modulation Spectra of Aircraft Blades," *IEEE National Radar Conference*, 1986, pp. 95–99.

[8]   Bullard, B. D., and P. C. Dowdy, "Pulse Doppler Signature of a Rotary-Wing Aircraft," *IEEE AES Systems Magazine*, May 1991, pp. 28–30.

[9]   Misiurewicz, J., K. Kulpa, and Z. Czekala, "Analysis of Recorded Helicopter Echo," *Proc. IEE Radar*, 1997, pp. 449–453.

[10] Andersh D. J., et al., "Xpatch: A High Frequency Electromagnetic-Scattering Prediction Code and Environment for Complex Three-Dimensional Objects" *IEEE Antennas and Propagation Magazine*, Vol. 6, February 1994, pp. 65–69.

[11] Bhalla, R., and H. Ling, "A Fast Algorithm for Simulating Doppler Spectra of Targets with Rotating Parts Using the Shooting and Bouncing Ray Technique," *IEEE Trans. on Antennas and Propagation*, Vol. 46, September 1998, pp. 1389–1391.

[12] Wang, Y., H. Ling, and V. C. Chen, "Application of Adaptive Joint Time-Frequency Processing to ISAR Image Enhancement and Doppler Feature Extraction for Targets with Rotating Parts," *SPIE Proc. on Radar Processing, Technology, and Application III*, Vol. 3462, pp. 156–163, 1998.

[13] Chen, V.C., "Radar Signatures of Rotor Blades," *SPIE Proc. on Wavelet Applications VIII*, Vol. 4391, 2001.